Journal of Iberian Geology (2023) 49:97–114
https://doi.org/10.1007/s41513-023-00210-0

RESEARCH PAPER

Geochemical distribution in residual soils of Iberian Pyrite Belt (Spain)

Iván Martín-Méndez[1,2] · Juan Llamas Borrajo[2] · Alejandro Bel-lan[1] · Juan Locutura[1]

Received: 5 May 2022 / Accepted: 23 March 2023 / Published online: 4 April 2023

Abstract

The Iberian Pyrite Belt (IPB) is a volcanic- and shale-hosted massive sulfides world-class province of the Upper Paleozoic age that includes some supergiant ore deposits with a unique mining operations history. An extensive soil (multi-element) geochemical survey in the IPB has been performed to create a geochemical database to increase the knowledge of the studied area. Both univariate and multivariate treatments have been done to manage a large amount of new data. The studied area shows higher background concentrations of several elements (e.b. Cu, Pb, Zn, Cd, Sn, In, Bi, As, or Sb) than in other terrains in Spain due to the IPB volcano-sedimentary ore deposits and their associated mining wastes. Mapping chemical elements help understand their behavior, controls and associations in natural environments. According to this, the mono-elemental contour maps show single-element distributions with geological control (e.g., Na), ore deposit control (e.g., Cu) or a mixture of both. On the other hand, multivariate analysis has been applied to reduce the large geochemical database maintaining the same information. We have chosen Factorial Analysis (FA) and obtained six factors that explain approximately 70% of the variability. Four of these factors (F1, F2, F4 and F5) show an intense geological control that improves the geological information of the IPB, while the other two (F3 and F5) show an ore deposit control. These factors allow distinguishing between different types of deposits in the IPB and help discover new possible exploration targets for future studies.

Keywords Geochemical mapping · Iberian Pyrite Belt · Mineral exploration · Soil

Distribución geoquímica en suelos residuales de la Faja Pirítica Ibérica (España)

Resumen

La Faja Pirítica Ibérica (FPI) es una provincia metalogenética de clase mundial de sulfuros masivos volcanosedimentarios de edad Paleozoico superior que incluye algunos yacimientos supergigantes que han sido explotado a lo largo de la historia. En este trabajo se ha llevado a cabo una campaña de geoquímica de suelos multielemental para crear una base de datos geoquímica que permita incrementar el conocimiento de la zona de estudio. Se han realizado tratamientos univariantes y multivariantes para interpretar la gran cantidad de nuevos datos generados. La zona muestra backgrounds más elevados para varios elementos (Ej: Cu, Pb, Zn, Cd, Sn, In, Bi, As o Sb) que en el resto de España debido a los yacimientos y a los residuos generados por su explotación. El mapeo de los elementos químicos ayuda a entender su comportamiento, su control y sus asociaciones en el medio natural. De acuerdo a esto, los mapas de contornos monoelementales muestran distribuciones de algunos elementos que presentan un control geológico (ej: Na), otros un monoelementales muestran distribuciones de algunos elementos que presentan un control geológico (ej: Na), otros un control metalogenético (ej: Cu) y otros una mezcla de ambos. Por otro lado, se han aplicado tratamientos multivariantes para reducir la gran cantidad de variables geoquímicas manteniendo la misma información. Hemos elegido el Análisis Factorial (AF) obteniendo 6 factores que explican aproximadamente el 70% de la varianza. Cuatro de esos factores (F1, F2, F4 y F5) muestran un claro control geológico que mejora la información geológica de la FPI, mientras que otros dos (F3 y F5) muestran un control metalogénico. Estos dos factores permites distinguir entre los diferentes tipos de yacimientos de la FPI y ayudan en el descubrimiento de posibles objetivos de exploración en futuros estudios.

✉ Iván Martín-Méndez
i.martin@igme.es

[1] Instituto Geológico y Minero de España (IGME-CSIC), Geología económica de los recursos minerales–GECOMIN, C/Ríos Rosas 23, Madrid, Spain

[2] E.T.S. Minas Madrid (UPM), Ríos Rosas 21, Madrid, Spain

1 Introduction

Geochemical mapping represents an application of conventional chemical methods to the knowledge of the natural environment (Plant et al., 1989). This is the most helpful way to determine the current levels of geochemical amounts—geochemical baselines—to comprehend the spatial distribution and variability of the different elements, and to document variations in their classes in natural materials at the Earth's surface (Demetriades et al., 2014). Those changes, usually shown in geochemical distribution maps, can often indicate areas affected by possible anthropic pollution activities or anomalies related to known or unsuspected mineralization.

Geochemical mapping is one of the main activities performed in national geological surveys and organizations. Following the recommendations in the Final Report of Project 259 for the International and National Geochemical Programs (Darlney et al., 1995), the Geological Survey of Spain achieved the Geochemical Mapping of Spain (Locutura et al., 2012). The main results accomplished with the data of the regional soil survey in the Iberian Pyrite Belt are presented below.

The IPB has been the scene of ancient mining activity since the Roman domination or even much earlier (Phoenicians or Tartessians). This proves several great mines that are still operating today. Further, they also show remnants of Roman extractive works (Pinedo-Vara, 1963). But the great leap forward for the mining activity in the IPB took place in the second half of the nineteenth century. Since then, there has been intense extractive and exploratory activity even when operations decreased, primarily because of the low price of the metals. Nowadays, the IPB continues to arouse unusual experimental interest, which indicates that the investment in this activity is still fruitful and profitable. One reason for this is the recent commissioning of five new mines or the enlargement of older ones that have started recently.

In the IPB study area, the recent past of intense exploration has been mostly based more and more on significant development and advance of the geological and metallogenetic processes, besides ground and airborne geophysical methods like gravimetric, electric, or electromagnetic methods. In contrast, geochemistry has yet to be applied to exploration projects. Yet, we can cite the geochemical survey carried out to assess the abundance and distribution of toxic trace elements in the soils of Andalusia, as relevant research has shown (Aguilar et al., 1999). This is because the suspected pollution associated with old mining has inhibited the application of geochemical techniques based on water, sediment, or rock samples, which are considered susceptible to easy contamination in those scenarios. Just a few local lithogeochemical surveys have been implemented (Díez-Montes et al., 2017), as well as applications of gas geochemistry (Bel-lán et al. unpublished). The only exception worth mentioning corresponds to the multi-elemental soil geochemistry study performed by SEIEMSA (Bonnemaison et al., 1993). This study used a multicriteria treatment with other geological and geophysical variables to define anomalies between the transect of the Herrerías mine and Puebla de Guzmán village, finding the small Vallejín pyrite deposit.

Finally, the recent literature shows different geochemical scientific studies related to the IPB, like Galán et al. (2008), that investigate the influence of geological setting on geochemical baselines of trace elements in soils in the South-West Spain. Further, Batista et al. (2012, 2020), also evaluated the mobility of trace elements from soils to sediments and geochemical exploration in the Portuguese part of the IPB, and Luz et al. (2014), used Cu, Zn, and Pb soil geochemistry for exploration. Likewise, Gonçalves and Mateus (2019) used data from stream sediments to delimitate several geochemical anomalies, and Fernández-Caliani et al. (2020) defined geochemical anomalies for some critical elements in soils of western Andalusia (Spain).

This study aims to create a new detailed and good-quality regional knowledge infrastructure of geochemical data from residual soils in the IPB. The main targets of this research are: (1) develop a geochemical database of residual soils from the IPB which increases the knowledge of the abundance and the spatial distribution of chemical elements; (2) determine the geochemical associations that govern the general variability, behavior and distribution of the elements by multivariate analysis; and (3) distinguish the main geochemical anomalies.

2 Geological setting

The study zone corresponds to the Spanish part of IPB that covers an area of about 3.000 km^2 in the Huelva and Seville provinces.

2.1 Regional geology

The Iberian Pyrite Belt (IPB) is a well-known area for its exceptional relevance and abundance of mineral deposits, extending around 230 km long and 40 km wide from Seville (Spain) to Lisbon (Portugal) (Quesada, 1996; Tornos, 2006) (Fig. 1A). It is located in the South Portuguese Zone, the southernmost of the six tectonic–magmatic zones defined by Julivert et al. (1974). This zone was sutured to the Hercynian massif during Dinantian-Namourian times, using the dismembered metamorphosed Acebuches ophiolite (Quesada, 1991).

The geology of the IPB has been studied by numerous authors (Inverno et al., 2015; Leistel et al, 1997; Quesada, 1996; Routhier et al., 1978; Schermerhorn, 1971; Strauss and Madel 1974; Tornos, 2006; among other). There is an

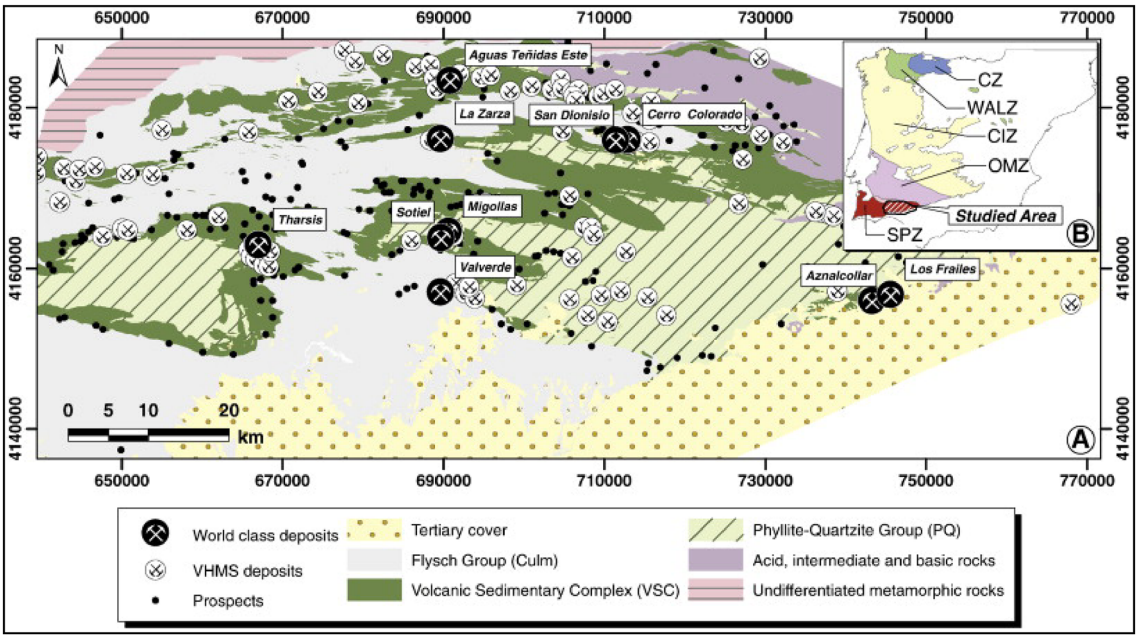

Fig. 1 **A** Geological schematic map of the Iberian Pyrite Belt from Gumiel et al. (2010)

agreement among most of the authors on the stratigraphic succession of the IPB, which consists of Upper Palaeozoic (Middle Devonian–Mississippian) sedimentary and igneous rocks that have been classically subdivided into three central lithostratigraphic units. From bottom (older) to top (younger) these are the Devonian Phyllite–Quartzite Group (PQ Group), the Late Devonian–Mississippian Volcano Sedimentary Complex (VSC) and the Late Visean–Moscovian post-volcanic succession (Culm Group).

One of the most significant features of the IPB is the great abundance of submarine volcanic processes giving place to continuous accumulations of volcanic and sedimentary materials with certain lateral continuity, forming a volcano-sedimentary pile or complex of hypabyssal, effusive, pyroclastic, and epiclastic-sedimentary rocks. Those materials of volcanic sources (Volcanic Sedimentary Complex, VSC), from late Devonian to Visean age, evolved along some volcanic phases, showing evidence of essential interactions with hydrothermal fluids from the volcanic or mixed volcanic-sedimentary origin, mobilized and activated by the most important thermal sources.

The PQ Group forms the base of the succession. It consists of a detrital sequence of shale and quartz-sandstone representative of shallow-water deposition, probably in a shallow marine platform (Mantero et al., 2011 and Moreno, 1993). There are two main outcrops: the eastern part of the Valverde del Camino antiform and the western part of la Puebla de Guzman antiform.

The VSC mainly comprises volcanic and subvolcanic rocks interbedded in a detrital sedimentary sequence of shales and volcano-derived sandstones. It is characterized by bimodal volcanism, with the presence of dacitic-rhyolitic dome complexes and sills, basaltic lava flows and sills, and thick pumice and crystal-rich felsic volcaniclastic units interbedded with detrital sedimentary rocks, mostly mudstone with some greywacke and sandstone (Leistel et al., 1997 and Tornos, 2006). In the'70s, Schermerhorn (1971) defined a synthetic column for the whole IPB with three different volcanic episodes, the first being the most relevant for the ore deposits.

The volcanic rocks mostly show a felsic composition ranging from dacite to rhyolite. Abundant albite, quartz phenocrysts, and minor biotite, partially or replaced by chlorite, appear in the rhyolitic rocks, which show perlitic and spherulitic textures. However, dacites show porphyritic textures (Rosa et al., 2010).

This is relevant to the study area, as outcrops with volcanic rocks of intermediate composition -andesites- only predominate in local parts of the northern IPB. These andesites are formed mainly by plagioclase, occasionally albitized, Fe-oxides, clinopyroxenes and rare quartz and biotite. Plagioclase are often altered to calcite, muscovite and epidote (Mitjavila et al., 1997).

In the upper part of the volcano-sedimentary sequence, there is a locally developed horizon, up to 30 m thick, of hematitic radiolaria-rich, purple-colored shale with Mn-bearing jasper lenses (Silva et al., 1990), called Manganesiferous Formation, which is an excellent stratigraphic reference level in the area.

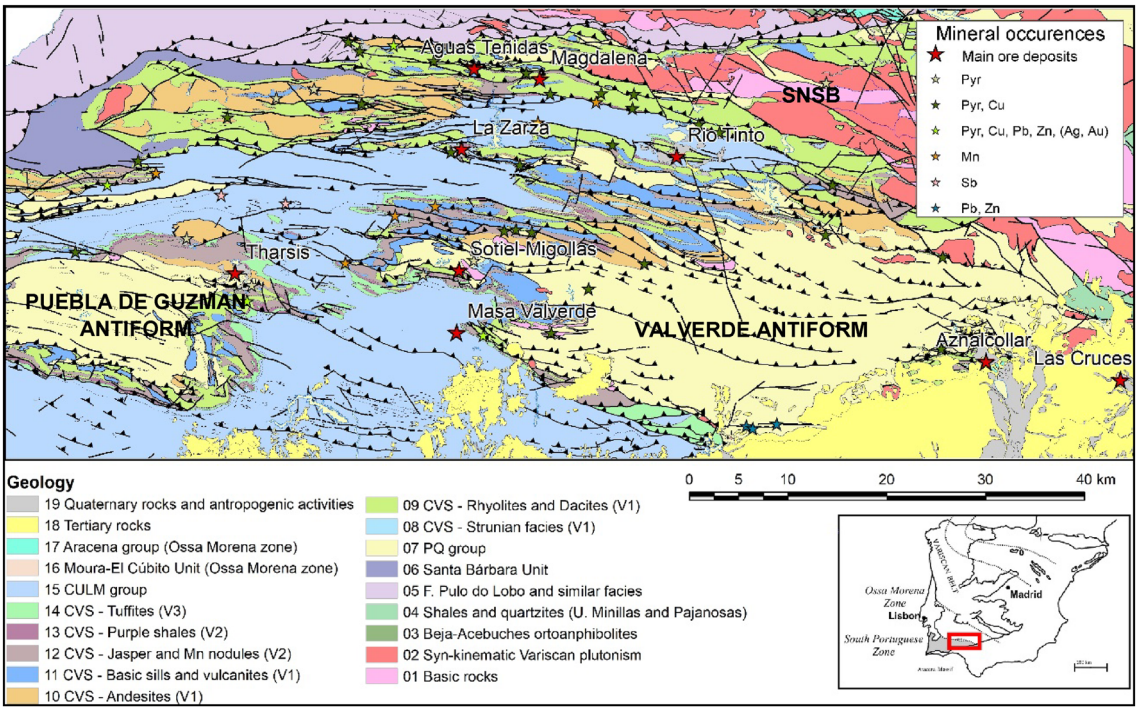

Fig. 2 Geological detailed map (modified from Matas et al., 2015) with mineral occurrences (García-Cortes, 2011)

Finally, towards the top, the VSC gradually evolves into the Culm group sequence, consisting of a synorogenic thick turbidite sequence of shales and sandstones that filled the foreland basin of the orogen (Leistel et al., 1997).

Plutonic rocks are confined to the northeastern part of the belt, forming the Sierra Norte de Sevilla Batholith (SNSB). This mass has diorites, tonalites and leucotonalites with a lesser proportion of gabbros, and granites (IGME, 1982; Schitz et al., 1987). The geochemical similarities between SNSB plutonic rocks and the materials of the volcanic successions (Díez-Montes and Bellido, 2008; Díez-Montes et al., 2011; Schütz et al., 1987; Thiéblemont et al., 1997), as well as the available U/Pb evidence (Dunning et al., 2002; Barrie et al., 2002) suggest that SNSB plutonic unit is genetically related with the VSC volcanic rocks.

The Pulo do Lobo sequence, in the northern part, consists of phyllites and quartzites that represents an accretionary complex developed in Variscan times and marks the SW Iberian suture, separating SPZ from the Ossa Morena Zone (OMZ) (Munhá et al., 1989; Pereira et al., 2008).

The north of the study area also crops out rocks that belong to the OMZ, and materials from the Guadalquivir Basin in the southeastern part (Fig. 2).

The current structure of the IPB represents the culmination of a complex process of cortical extension and associated magmatism that was produced by the oblique collision of the continental block of the SPZ with the active margin of the Iberian block located to the north and which ended with the obduction of the latter on that of the SPZ (Almodóvar et al., 2019; Leistel et al., 1997).

2.2 Mineral deposits

The Iberian Pyrite Belt is one of the most significant accumulations of metals contained in volcanogenic massive sulfide (VMS) deposits worldwide (Almodóvar et al., 2019; Leistel et al., 1997) with more than 80 known deposits containing > 1700 Mt of sulfide ore (mined and reserves), and some tens of Mn occurrences (Fig. 2).

Different types of mineral deposits in the IPB include mineralization in VMS, stockworks, gossans and Cu-rich shales. Mn is also extracted from small open pits linked to hydrothermal mineralizations and volcanism (Locutura, 2011).

More than 80 ore deposits and 100 mineral occurrences are located within the studied area in the IPB. We can highlight some of the VMS ore deposits over 50 Mt (e.g.

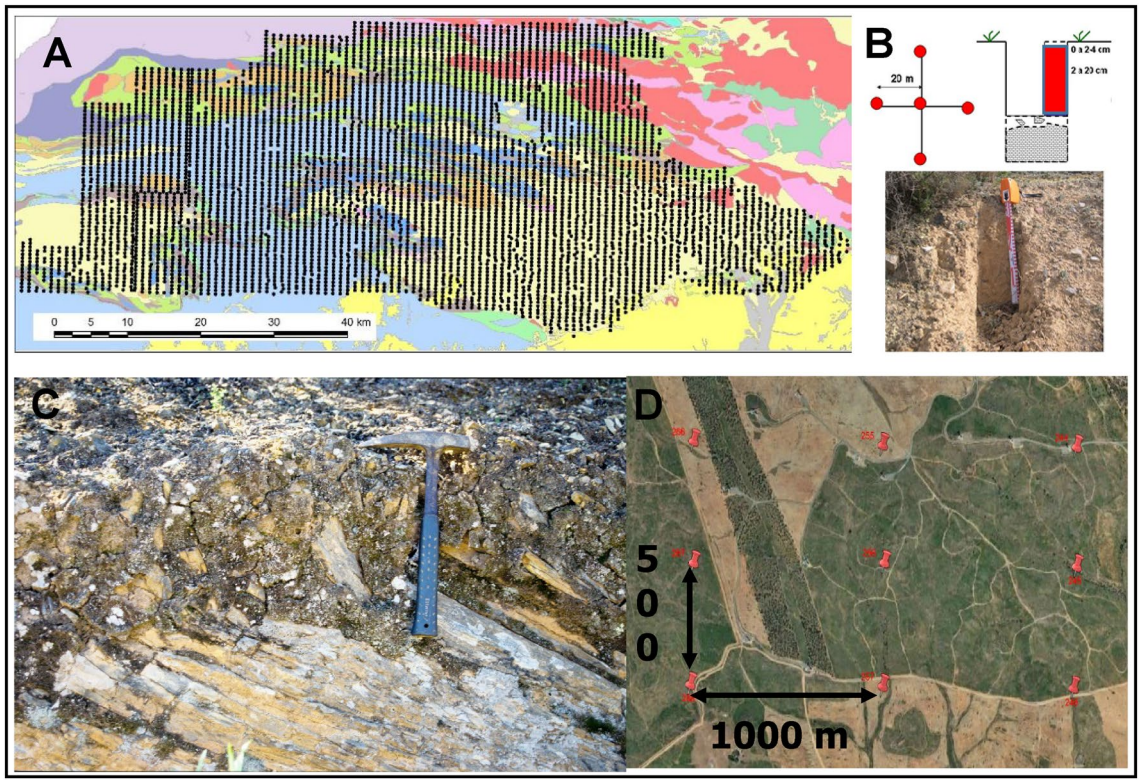

Fig. 3 **A** Distribution of 6197soil samples in the study area. **B** Diagram of composite sampling method and sampling soil profile. **C** Soil example of the study area. **D** Grid of sampling 500 m × 1000 m under satellite view

Rio Tinto, La Zarza, Tharsis, Aznalcollar-Los Frailes, Sotiel-Migollas, Masa Valverde and Aguas Teñidas) and the most important Mn ore, Soloviejo.

Nowadays, mining companies are working in Aguas Teñidas, La Magdalena, Río Tinto and Sotiel-Migollas deposits. This illustrates the great mining importance of the area with tonnages greater than 50 Mt. Another active mine in the area is Las Cruces, which is working a blind orebody of Cu-rich minerals under 120 m of Tertiary marls covering, in the alluvial plain of the Guadalquivir River, near Seville. The initial reserves of this deposit were 17.2 Mt grading 6.2% Cu in the secondary enrichment zone and some additional resources in the primary mineralization and the gossan (Yesares et al., 2015).

3 Material and methods

3.1 Sampling and sample preparation

The type of sample selected for the geochemical mapping of the study zone was residual soil, which followed the recommendations of the Geochemical Baseline Program (Salminen, et al. 1998).

During the field campaign from spring 2016 to spring 2017 were collected up to 6197 soil samples, at an average sampling density of two samples per km^2 (a grid of 500 × 1000 m) in N-S profiles, and an average weight of 3 kg. They were taken from 2 to 20 cm depth when possible due to the poor development of soils in the Pyrite Belt. Most of the sampled soils are classified Leptosols (WRB, 2014). These soils rarely reach more than 10–20 cm above bedrock. This is why they show bedrock fragments and low contents of new formation minerals, clays and Mn and Fe hydroxides (Fernández-Caliani et al., 2009) (Fig. 3C).

Samples were collected as composite samples from five pits within 100 m^2 (Fig. 3B) (Locutura et al., 2012). Soil samples were firstly sieved to < 3 mm during the field campaign. For quality control purposes, a field duplicate was taken at every 30 sample site, with an offset distance of ca. 10–20 m from the original sample site.

All samples were shipped to a central sample preparation facility at the Geological Survey of Spain (IGME). All samples were processed by the protocol described by Salminen et al. (2005). Each sample was oven dried at 40 °C, followed by break up, homogenization and, finally, split into sub-samples. Soil samples passed through a 100 mesh nylon screen (150 µm). Before sending the samples to laboratory, all of them were randomized, and analytical replicates

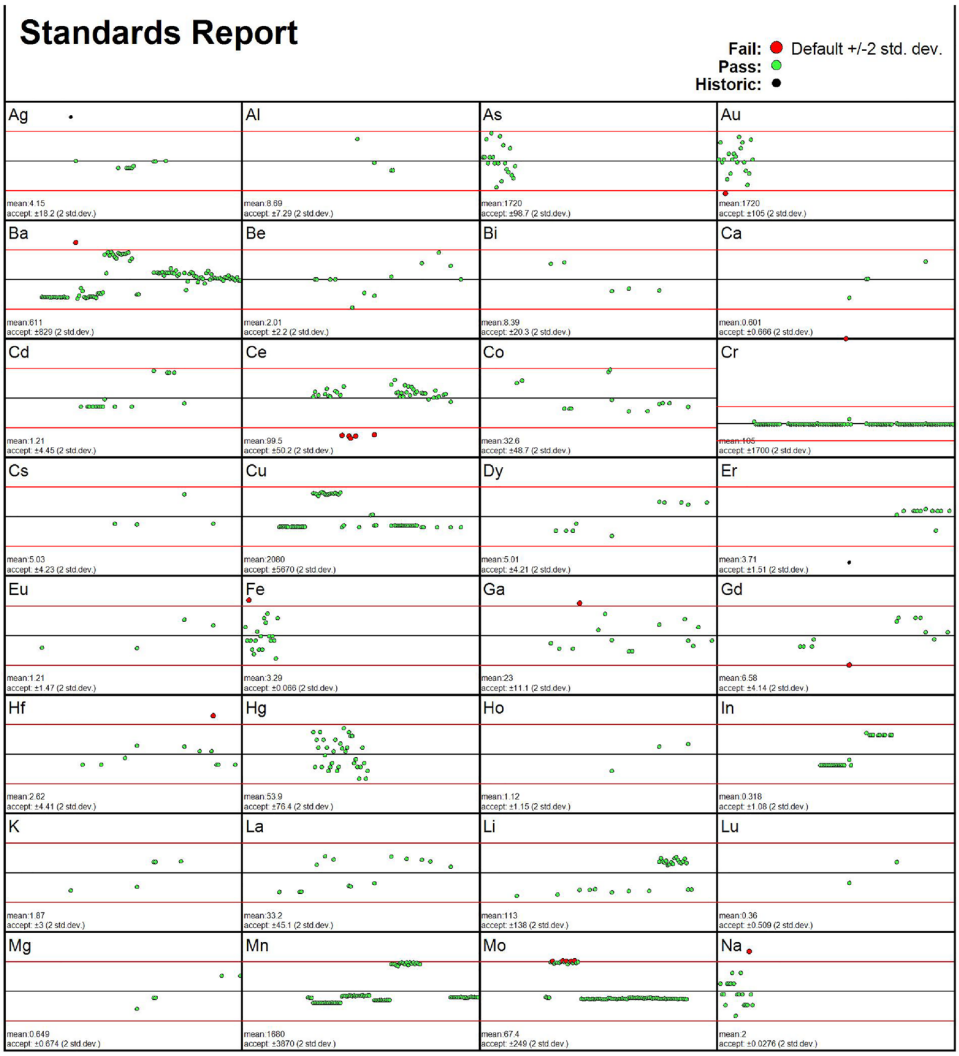

Fig. 4 Quality control report from some elements from Actlabs Laboratories (international standard materials)

prepared from the field duplicates, following the procedure of Locutura et al. (2012).

3.2 Chemical analyses and quality control

Chemical analyses of 64 elements were carried out at Actlabs Laboratories Ltd. (Ontario, Canada), after a tetra-acid digestion, by a combination of inductively coupled plasma atomic emission spectroscopy (ICP-AES) (Al, Ca, K, Mg, Mn, Mo, Na, P, S, Ti and V), inductively coupled plasma mass spectrometry (ICP-MS) (Ag, Ba, Be, Bi, Cd, Co, Cr, Cs, Cu, Ga, Ge, Hf, Hg, In, Li, Nb, Ni, Pb, Rb, Re, Se, Sn, Sr, Ta, Te, Th, Tl, U, Y, Zn, Zr, La, Ce, Pr, Nd, Sm, Eu, Gd, Dy, Tb, Ho, Er, Tm, Yb and Lu) and instrumental neutron activation analysis (INAA) (As, Au, Br, Fe, Hf, Ir, Na, Sb, Sc, W, La, Ce, Nd, Sm, Eu, Tb, Yb and Lu).

Chemical element concentrations were determined using a tight internal and external quality control procedure. Quality control of the analytical approach included using a method reagent blank, duplicates, and certified reference materials to ensure the accuracy and precision of results. The relative deviations of the standard analyses to the reference values were typically below 10%. The internal quality control (IQC) in Actlabs Laboratories Ltd. was based on introducing into the batches of an international standard material each 10–15 samples (Fig. 4). The results showed no systematic errors or instrumental deviations (less than 100% ± 2 standard deviation) of these quality control supplies by the laboratory.

External quality control (EQC) was based on (a) a field duplicate taken at a rate of 1 in 20 samples, which can determine the sampling variance, sampling preparation variance, and analytical variance. The variation in the EQC is larger than in the IQC due to the sum of the different variances. We have defined a confidence band of 25%, which almost all elements fit. Nevertheless, elements with a variation range close to the lower detection limit (Ag, Au, Bi, Cd, Ge, Hf,

Table 1 Statistical parameters for major, minor and trace elements in the IPB soils (6194 samples, 0–20 cm horizon, analyzed by ICP-MS, ICP-AES or INAA, Det. Lim: laboratory detection limit, P: Percentil, < BDL: Below detection limit

Element	An. Tecnic.	Det. Lim.	Medium	Median	Minimun	Maximun	P.90	P.97,5	Variance	Stand. Dev.	Var. Coef.
Ag (mg/kg)	ICP-MS	0.05	0.27	0.14	< BDL	83	0.36	0.83	2.559	1.6	5.932
Al (%)	ICP-AES	0.01	8.72	8.79	0.01	16.1	11.20	12.4	3.99	1.997	0.229
As (mg/kg)	INAA	0.5	41.75	28.65	< BDL	3460	59.30	134	10,263.718	101.31	2.427
Au (µg/kg)	INAA	2	9.37	< BDL	< BDL	3400	19	38	3247.038	56.983	6.081
Ba (mg/kg)	ICP-MS	1	406.58	382	< BDL	16,200	654	852	112,671.807	335.666	0.826
Be (mg/kg)	ICP-MS	0.1	2.31	2.4	< BDL	8.9	3.4	3.9	0.778	0.882	0.381
Bi (mg/kg)	ICP-MS	0.1	1.10	0.6	< BDL	328	1.60	3.9	29.305	5.413	4.93
Br (mg/kg)	INAA	0.5	5.11	5	< BDL	37.9	9.70	13.9	15.17	3.895	0.762
Ca (%)	ICP-AES	0.01	0.64	0.15	0.01	19.7	1.90	4.11	2.109	1.452	2.258
Cd (mg/kg)	ICP-MS	0.1	0.12	0.05	< BDL	31.2	0.20	0.4	0.181	0.426	3.549
Co (mg/kg)	ICP-MS	0.1	19.13	19	< BDL	108	31.70	42.6	113.283	10.643	0.556
Cr (mg/kg)	ICP-MS	1	88.35	88	< BDL	2140	128	215	3648.256	60.401	0.684
Cs (mg/kg)	ICP-MS	0.05	6.91	5.81	< BDL	74.5	14.70	22.3	33.583	5.795	0.838
Cu (mg/kg)	ICP-MS	0.2	59.57	43.7	3.70	3890	95.50	221	10,286.48	101.422	1.702
Fe (%)	INAA	0.01	4.01	4.11	0.39	24.4	5.45	6.66	1.807	1.344	0.335
Ga (mg/kg)	ICP-MS	0.1	20.04	20.1	2	40.5	26.90	30.3	27.926	5.285	0.264
Ge (mg/kg)	ICP-MS	0.1	0.31	0.2	< BDL	2.6	0.70	1.1	0.091	0.301	0.982
Hf (mg/kg)	ICP-MS	0.1	6.67	6	< BDL	38	11	16	14.036	3.746	0.562
Hg (µg/kg)	ICP-MS	10	86.54	40	< BDL	15,700	140	300	164,871.526	406.044	4.692
In (mg/kg)	ICP-MS	0.1	0.08	< BDL	< BDL	24	0.10	0.2	0.107	0.327	4.256
Ir (mg/kg)	INAA	5	< BDL	< BDL	< BDL	< BDL	< BDL	< BDL	0	0	0
K (%)	ICP-AES	0.01	1.95	1.98	0.01	4.85	3.01	3.49	0.698	0.836	0.428
Li (mg/kg)	ICP-MS	0.5	55.36	50.2	3.3	400	95.70	137	1292.216	35.947	0.649
Mg (%)	ICP-AES	0.01	0.54	0.43	0.01	5.26	0.94	1.73	0.177	0.421	0.783
Mn (mg/kg)	ICP-AES	1	966.21	807.5	< BDL	26,700	1760	2800	707,798.979	841.308	0.871
Mo (mg/kg)	ICP-AES	1	0.81	0.5	< BDL	31	2	3	0.892	0.945	1.166
Na (%)	INAA	0.01	0.87	0.53	0.03	5.02	2.08	3.02	0.613	0.783	0.898
Nb (mg/kg)	ICP-MS	0.1	1.48	0.2	< BDL	30.6	4.60	12.8	10.178	3.19	2.153
Ni (mg/kg)	ICP-MS	0.5	35.30	35.1	< BDL	943	55	79.8	760.045	27.569	0.781
P (%)	ICP-AES	0.001	0.04	0.036	0.001	0.42	0.06	0.077	0	0.019	0.511
Pb (mg/kg)	ICP-MS	0.5	63.50	37.2	3	5000	87.70	229	44,272.843	210.411	3.313
Re (mg/kg)	ICP-MS	0.001	0.003	0.001	0.001	1.16	0.01	0.012	0	0.019	7.36
S (%)	ICP-AES	0.01	0.02	0.02	0.01	1.25	0.03	0.05	0.001	0.038	1.85
Sb (mg/kg)	INAA	0.1	6.32	3	< BDL	3020	7.20	16.7	2929.562	54.125	8.567
Sc (mg/kg)	INAA	0.1	16.48	16.3	1.4	53.5	22.5	31.7	34.533	5.877	0.357
Se (mg/kg)	ICP-MS	0.1	0.756	0.6	< BDL	56.7	1.5	2.3	2.084	1.444	1.91
Sn (mg/kg)	ICP-MS	1	1.877	1	< BDL	200	4	7	27.168	5.212	2.777
Sr (mg/kg)	ICP-MS	0.2	88.509	76.9	6	721	147	228	2847.842	53.365	0.603
Ta (mg/kg)	ICP-MS	0.1	0.103	0.05	< BDL	2.3	0.2	0.8	0.037	0.191	1.857
Te (mg/kg)	ICP-MS	0.1	0.078	0.05	< BDL	1.6	0.1	0.4	0.011	0.104	1.339
Th (mg/kg)	ICP-MS	0.1	14.233	15.1	< BDL	56.6	20.7	23.8	31.057	5.573	0.392
Ti (%)	ICP-AES	0.01	0.244	0.21	< BDL	1.19	0.44	0.61	0.021	0.145	0.593
Tl (mg/kg)	ICP-MS	0.05	0.701	0.67	< BDL	30.6	1.05	1.42	0.653	0.808	1.154
U (mg/kg)	ICP-MS	0.1	2.829	2.9	< BDL	9.7	3.8	5.1	1.159	1.077	0.38
V (mg/kg)	ICP-AES	2	67.786	63	< BDL	302	119	150	1403.758	37.467	0.553
W (mg/kg)	INAA	1	0.846	0.5	< BDL	149	0.5	3	14.262	3.777	4.466
Y (mg/kg)	ICP-MS	0.1	22.02	19.8	3.1	77.5	33.7	44.6	72.073	8.49	0.386
Zn (mg/kg)	ICP-MS	0.5	83.317	72.9	7.9	7700	121	210	13,729.742	117.174	1.406
Zr (mg/kg)	ICP-MS	1	87.117	83	2	475	145	192	2394.997	48.939	0.562

Table 1 (continued)

Element	An. Tecnic.	Det. Lim.	Medium	Median	Minimun	Maximun	P.90	P.97,5	Variance	Stand. Dev.	Var. Coef.
La(mg/kg)	ICP-MS	0.1	42.005	42.4	0.9	201	66.4	82.8	397.528	19.938	0.475
Ce (mg/kg)	ICP-MS	0.1	88.906	89.4	2.9	415	140	172	1660.372	40.748	0.458
Pr (mg/kg)	ICP-MS	0.1	10.224	10.2	0.5	49.8	16.1	20	22.103	4.701	0.46
Nd (mg/kg)	ICP-MS	0.1	38.422	38.2	2.5	179	59.5	74.8	286.558	16.928	0.441
Sm (mg/kg)	ICP-MS	0.1	7.282	7.05	0.6	31.6	11.1	13.9	8.94	2.99	0.411
Eu (mg/kg)	ICP-MS	0.05	1.403	1.38	0.1	6.07	2.07	2.57	0.284	0.533	0.38
Gd (mg/kg)	ICP-MS	0.1	5.886	5.6	0.6	20.9	8.4	10.6	4.061	2.015	0.342
Dy (mg/kg)	ICP-MS	0.1	4.572	4.2	0.5	17	6.5	8.7	2.437	1.561	0.341
Tb (mg/kg)	ICP-MS	0.1	0.788	0.8	<BDL	2.6	1.1	1.4	0.063	0.251	0.319
Ho (mg/kg)	ICP-MS	0.1	0.893	0.8	0.1	3.6	1.3	1.8	0.116	0.34	0.381
Er (mg/kg)	ICP-MS	0.1	2.635	2.4	0.3	10.6	4	5.4	1.044	1.022	0.388
Tm (mg/kg)	ICP-MS	0.1	0.399	0.4	<BDL	1.5	0.6	0.8	0.024	0.156	0.392
Yb (mg/kg)	ICP-MS	0.1	2.57	2.3	0.4	9.6	3.6	5.3	0.842	0.917	0.357
Lu (mg/kg)	ICP-MS	0.1	0.409	0.4	<BDL	1.6	0.6	0.9	0.023	0.151	0.37

Hg, In, Mo, Re, S, Se, Sn, Ta, Te and W) and elements that appear in refractory minerals (Ti, V and Zr) show higher but acceptable errors. The quality control follows the descriptions in Demetriades et al. (2014).

3.3 Statistical analysis

A complete database with all analytical results, data from field campaigns and other outstanding characteristics were prepared for statistical computation, based on Reiman et al. (2008). The element concentrations below the instrumental detection limit (IDL) have been assigned a value corresponding to half their detection limit. The results of the chemical analyses were processed using STATISTICA software to generate the statistical parameters used to guide the interpretation of the results.

3.3.1 Univariate statistical analysis and spatial distribution

Univariate statistical analyses were performed to show the single-element geochemical distribution. The spread of element concentration values, distributions and identification of multiple populations and outliers, were examined through calculations of different parameters summarized in Table 1. Also, deviations from normal or log-normal behavior were investigated for each element (Reiman et al., 2005). The representation of the populations of the different elements in the form of histograms and box plots has made it possible to observe that some trace elements deviate from the normality patterns. Spatial distribution maps of the chemical elements have been made by interpolating the inverse of the weighted distance (ID^2). The main features of element geochemical distributions through point maps and contour maps can display possible relationships with geologic features (Reiman, 2005). The interpolation grid was defined by a cell of 800 m (x axis) and 400 m (y axis), in accordance with the sampling grid. The radio search (anisotrope) was 3000×2000 m with a direction of N110E. Contours maps were generated using ArcGIS software and statistical percentiles (10th, 25th, 50th, 75th, 90th and 97.5th).

3.3.2 Multivariate treatment

Multivariate statistics is a valuable tool for treating geochemical data in geochemical surveys, as it allows investigating several variables and their interactions simultaneously. There are different options for multivariate treatment in geochemical exploration including principal component analysis (PCA), factor analysis (FA), independent component analysis, cluster analysis and multidimensional scaling (Zuo et al., 2021).

According to Grunsky (2010), PCA and FA are the most popular multivariate techniques for managing geochemical exploration data because these techniques reduce many elements into several factors based on the correlation between variables. We have used FA between these two options because PCA accounts for a maximum variance of all variables, so all variables have to enter into the factor and show the total structure in the data (all variables are "forced" into the result and in contrast, FA is based on the correlation structure of the variables and factors do not have to explain the total variation of the data, there are unusual variables will not enter the common factors (Reiman et al., 2002).

4 Results and discussion

4.1 Univariate spatial distribution

The spatial distribution of a chemical element in a given area can be of various types or forms. The high values, those of the intermediate range and the very low ones can be adjusted approximately well, to the contours of geological or lithological units. These guidelines reflect a special relationship between the unit above and the element that can define the unit, for example, Na in the IPB. Another form of distribution is one in which the values of the element bear no relation whatsoever to the contours of the units or the geological structure, but rather appear with an uneven distribution, in small (or intermediate) spots of color (range of generally high or very high) scattered, cutting contours. However, this distribution may be more accentuated in some geological enclosures than others. This distribution modality can result from existing mineralization elements mobilized by secondary or primary geochemical dispersion. Depending on the nature of the element, they can also be associated with industrial or agricultural pollution, for example, Cu in the IPB. Finally, some elements present mixed distribution patterns with characteristics of the two previous distribution models. They usually occur in the case of trace elements uniformly distributed in a lithology or unit that can be mobilized to a certain degree in the regional context, producing a distribution pattern adjusted to a unit and, at the same time, an erratic dispersion outside it (Reiman, 2005).

Sodium is a metal with a litophile affinity. It forms its own minerals: silicates like albite ($Na_2AlSi_3O_8$), chlorines like halite (NaCl), carbonates like sosa (Na_2CO_3), and fluorides like criolite (Na_3AlF_4). However, this element is more common in minerals that form rocks, and it appears included in its crystallographic structure, both in form of the trace element and important components. For example, silicates, like feldspars, sodium micas, amphiboles and pyroxenes. Its natural associations are Cl, Na, Mg, Br, S, its relationship with marine breezes and inputs, and with brines and evaporitic environment. Other natural associations are Si, Al, Na and K, related to acid igneous rocks. Sodium increases its concentration in magmatic differentiation processes from basic to acid rocks, so, it presents a higher concentration in this type of igneous rocks (Locutura et al., 2012).

Sodium Clarke's is 2.27% (Taylor, 1964) and in soils Na_2O median amount is estimated 1.3%. In the European Union, the average in soils is 0.8% (Salminen et al., 2005),

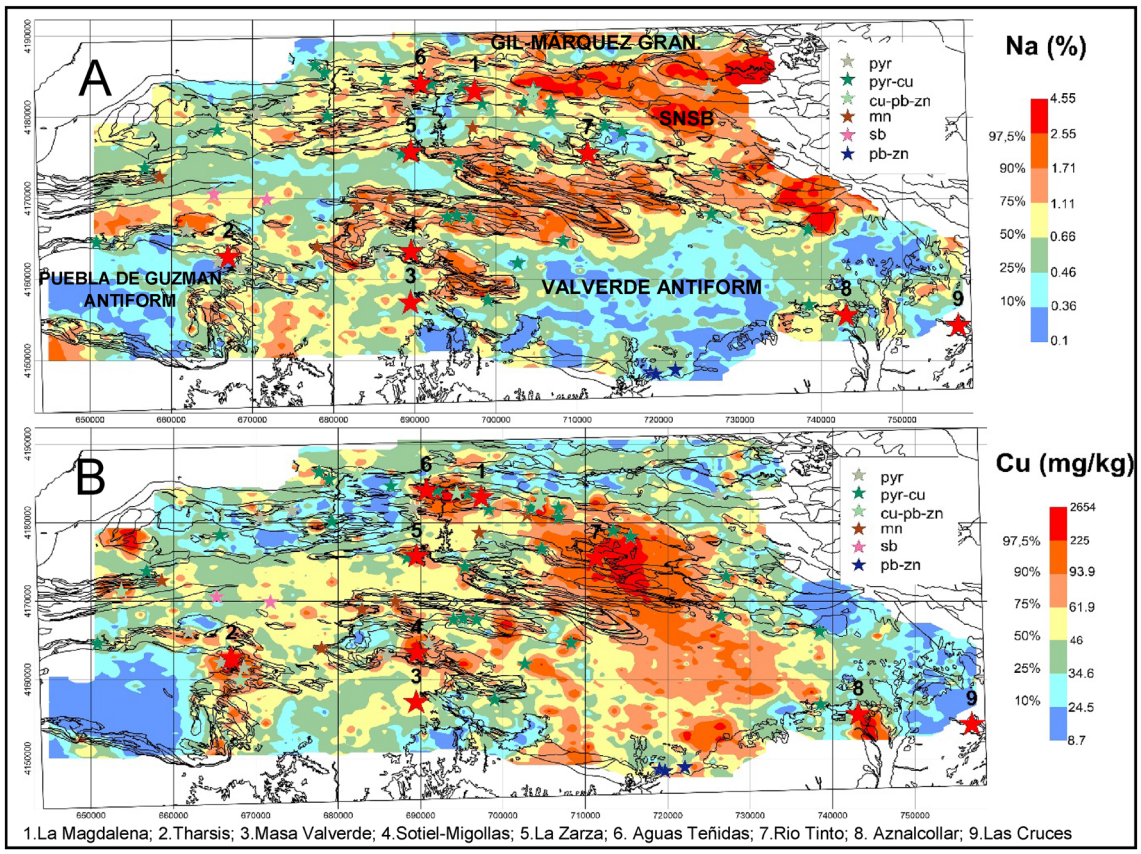

Fig. 5 **A** Monoelemental contour map of sodium (Na). **B** Monoelemental contour map of copper (Cu)

while in Spain is 0.31% (Locutura et al., 2012), all of these results were measured on the fraction < 2 mm.

In our studied zone for the fraction < 150 µm, Fig. 5A sodium median contents in soils are 0,53% and Na_2O median contents are 0,71%, higher than the average contents of Spain, 0.87%. This is due to the higher values of the VS complex (up to 1%), with a high quantity of acid rocks that increase the baseline of the entire zone. Sodium clearly distinguishes the northwest igneous rocks, with higher values (up to 2%) in the acid units (Variscan granites) and the VS complex; the volcanism shows compositions from basalt to rhyolite. However, the most felsic terms dominate, as domes and sills are associated to volcanoclastic deposits with similar chemical composition.

Copper is a metal with a high chalcophile affinity. It forms a broad group of its minerals, like sulfides, sulfur-antimonides, sulfo-arsenides, carbonates, and oxides, the most frequent being chalcopyrite ($CuFeS_2$), chalcocite (Cu_2S), bornite (Cu_5FeS_4), covelline (CuS), cuprite (Cu_2O), malaquite and azurite, but also native copper. Therefore, it appears in the crystal lattice of silicates (biotite, pyroxenes and amphiboles and of sulfides (sphalerite and oxides (magnetite) in substitution of Fe or Mg, so, it is more abundant in basic igneous rocks than acid igneous rocks (Locutura et al., 2012).

Copper Clarke's is 68 mg/kg (Mielke, 1979) and in soils the median content of Cu is between 13 and 24 mg/kg (Kabata-Pendias, 2001). For the EU the median content in soils is 13 mg/kg (Salminen et al., 2005); in Spain, the median content in soils is 18.5 ppm and finally, the median content in Andalucía soils is 24 mg/kg (Locutura et al., 2012), all of these results was measured on the fraction < 2 mm. Copper can be relatively immobile in soils but its fixation processes (adsorption, occlusion and co-precipitation, organic chelation and complexing, microbial fixation), among other soil parameters, can be controlled by pH (Kabata-Pendias, 2001).

In the study area for the fraction < 150 µm, (Fig. 5B) Cu median content in soils, 43.7 mg/kg, are higher than the medium contents worldwide, Europe, Spain and Andalusia. This is due to the vast quantity of Cu-rich sulfur deposits. The area's central part, mainly made up of materials from the Volcano-Sedimentary Complex, contains a dispersion of minor anomalies, related to the numerous existing deposits on a yellow background (40–60 mg/kg). However, in most peripheral areas, with limited deposits and more sterile lithologies (PQ Group and Culm), the Cu backgrounds are lower (less than 35 mg/kg) and with a completely uneven distribution. Also, we can observe a high and wide anomaly in the IPB with values of 56.5 mg/kg or even higher. More significant abnormalities are related to the more enormous ore deposits in this zone, like La Zarza, Sotiel, Aguas Teñidas, Cueva de la Mora, San Telmo, Tharsis, and Rio Tinto, there are other anomalies unrelated to already known deposits and so, with a prospective interest.

4.2 Multivariate spatial distribution

Factor analysis was used to investigate the complex multivariate relationships among variables. The treatment aims to explain the variation in an extensive database by as few "factors" as possible. Factor analysis served to identify different groups of chemical elements with approximately the same geochemical pattern. However, FA is sensitive to outliers in the data, so it needs a normal distribution of the population before carrying out a classical FA (Reiman et al., 2002).

We have made several attempts to change the number of factors and elements. We have finally chosen the normal population instead of the log transformation population because we have deleted the extreme values and outliers with

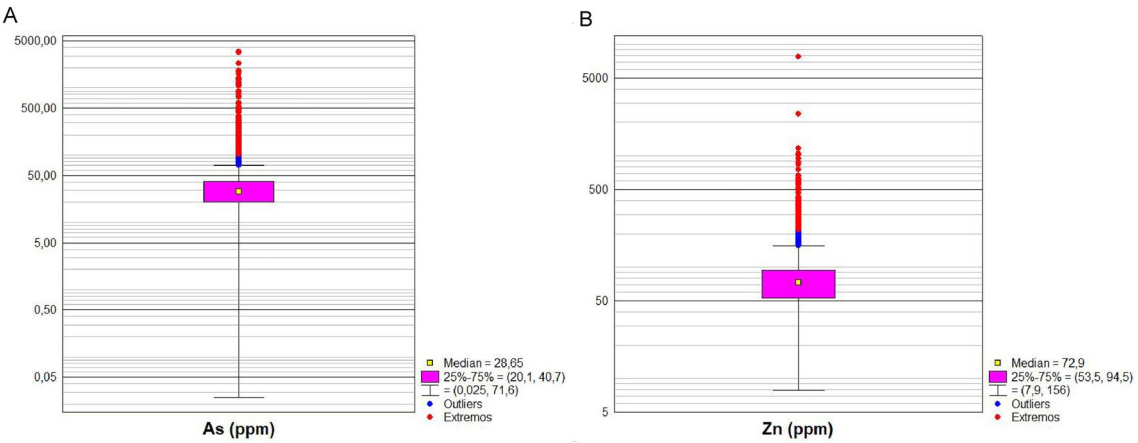

Fig. 6 **A** As a Box plot of the total population of samples with outliers (blue) and extremes (red). **B** Zn Box plot of the total population of samples with outliers (blue) and extremes (red)

Table 2 Varimax rotated factors (six-factor model) for 6194 soils samples from IPB

	Factor 1	Factor 2	Factor 3	Factor 4	Factor 5	Factor 6
Au	-0.0394	-0.0001	**0.9148**	0.0095	0.0340	0.0369
Ag	-0.0360	0.0153	**0.8214**	-0.0144	0.4041	0.0046
Cu	0.0525	0.0495	0.2957	0.1268	0.4813	0.0345
Cd	-0.0451	0.0300	0.0283	0.0303	**0.8730**	-0.0228
Pb	-0.0076	0.0067	**0.7333**	0.0006	0.4813	-0.0018
Ni	0.0490	-0.0863	-0.0197	**0.6892**	0.0268	0.1286
Zn	0.0327	0.0153	0.0429	0.1166	**0.8731**	0.0125
S	-0.0294	-0.0326	0.3311	0.1015	**0.5368**	-0.0668
Al	**0.6583**	0.0218	-0.0280	**0.5698**	-0.0188	0.1051
As	0.0828	0.0074	**0.8061**	0.0399	0.2659	-0.0227
Ba	0.4042	-0.0088	**0.6342**	0.0464	0.1116	0.1074
Be	**0.8448**	0.0756	0.0123	0.1500	0.0074	0.2157
Bi	-0.0307	0.0247	**0.9591**	0.0039	0.0175	0.0125
Br	0.0632	-0.2248	-0.0129	0.1645	0.0315	0.0392
Ca	**-0.5277**	0.0139	-0.0384	0.2410	0.0407	-0.1286
Co	0.1306	-0.0896	-0.0092	**0.7709**	0.0312	0.1797
Cr	-0.0389	-0.1449	-0.0271	**0.7440**	0.0246	0.0203
Cs	**0.6529**	-0.1937	0.0119	0.1642	-0.0050	0.1383
Fe	0.1101	-0.0585	0.2423	**0.8296**	0.1067	0.0848
	Factor 1	**Factor 2**	**Factor 3**	**Factor 4**	**Factor 5**	**Factor 6**
Ga	**0.7225**	0.1142	0.0218	0.4950	-0.0018	0.1075
Hg	0.0187	0.0222	0.2621	-0.0226	**0.5193**	-0.0182
In	-0.0273	0.0141	0.1909	0.0086	0.3053	0.0822
K	**0.8249**	-0.0934	0.0257	0.0289	0.0245	0.1895
Li	**0.5930**	-0.2251	-0.0012	0.3162	-0.0258	0.1603
Mg	-0.4551	0.2480	-0.0449	**0.5900**	0.0520	-0.1224
Mn	0.0154	0.1242	-0.0226	0.3755	0.0309	0.1369
Na	**-0.5026**	0.3682	-0.0559	0.0694	-0.0596	-0.3086
P	0.1861	-0.1357	0.1058	0.4962	0.1281	0.1795
Rb	**0.8347**	-0.0923	0.0250	0.0318	0.0306	0.2070
Sb	-0.0408	-0.0072	**0.8408**	-0.0137	0.3084	0.0251
Sc	-0.1101	0.0907	-0.0541	**0.8312**	-0.0092	-0.0777
Sn	0.1125	0.0767	**0.7445**	-0.0061	0.0256	-0.0265
Sr	-0.3020	0.0717	-0.0370	**0.5232**	0.0067	-0.1054
Th	**0.7977**	-0.0057	0.0365	-0.1139	-0.0276	0.3560
Tl	0.4386	0.0300	0.2383	0.0279	0.4228	-0.0197
U	**0.6384**	0.0640	0.0405	-0.2429	0.0434	0.2646
V	0.2774	-0.2066	0.0641	**0.6254**	0.0569	0.0173
Y	-0.1654	**0.9622**	0.0142	0.0419	0.0277	0.0228
La	**0.5939**	-0.0584	0.0298	0.0503	-0.0032	**0.7811**
Ce	**0.6034**	-0.0345	0.0240	0.0493	-0.0046	**0.7681**
Pr	**0.5562**	-0.0158	0.0253	0.0796	-0.0001	**0.8146**
Nd	**0.5357**	0.0101	0.0217	0.0950	0.0006	**0.8237**
Sm	0.4815	0.1253	0.0209	0.1340	0.0090	**0.8322**
Eu	0.3026	0.1079	-0.0024	0.4627	0.0150	**0.7706**
Gd	0.2968	**0.5109**	0.0250	0.2226	0.0397	**0.7411**
Dy	-0.0662	**0.9431**	0.0183	0.1260	0.0377	0.2250
Tb	0.0832	**0.8051**	0.0230	0.1927	0.0417	**0.5025**
Ho	-0.1360	**0.9712**	0.0169	0.0601	0.0361	0.0576
Er	-0.1121	**0.9830**	0.0171	-0.0172	0.0283	-0.0059
Tm	-0.0402	**0.9699**	0.0214	-0.0850	0.0225	-0.0271
Yb	0.0318	**0.9464**	0.0220	-0.1755	0.0164	-0.0437
Lu	0.0746	**0.9141**	0.0225	-0.1983	0.0132	-0.0437
Expl.Var	8.0496	7.8581	5.7432	5.7693	3.2186	5.3606
Prp.Totl	0.1548	0.1511	0.1104	0.1109	0.0619	0.1031

F1 = Be-Rb-K-Th-Al-U-Li-(Ba-Sm-Tl-Eu-Gd-V) in contrast to Ca-Na-(Mg-Sr); F2 = Er-Ho-Tm-Y-Yb-Dy-Lu-Tb-Gd-(Na); F3 = Bi-Au-Sb-Ag-As-Sn-Pb-Ba-(S-Cu-Hg); F4 = Fe-S-Co-Cr-Ni-V-Al-Sr-(P-Ga-Mn-Li); F5 = Cd-Zn-S-Hg-(Cu-Pb-Tl-Ag-Sb-In-As); F6 = Sm-Nd-Pr-La-Eu-Ce-Gd-Tb-(Th-U) in contrast to (Na). Pale green: loading values between 0.25 and 0.5; Green: loading values over 0.5; Pale red loading values between -0.25 and -0.5; Red: loading values under -0.5

the help of the representation of the populations in box plots (Fig. 6A, B examples), which has allowed us to differentiate them which have been eliminated for this multivariate treatment. We have noted a higher consistency of the results with this treatment in the normal population. This solution accounts for 69.22% of the total variance.

The different factors obtained were studied and interpreted by their hypothetical origin (natural, anthropogenic, or mixed). ArcGis software has been used for producing color surface maps showing element and association factor score distributions. Maps of factor score distributions are handy to correlate lithological units with physicochemical and pollution processes of the surface environment at each sampled site (Reiman et al., 2002). Inverse distance weighted (MIDW) is the interpolation method with the same parameters as contours maps.

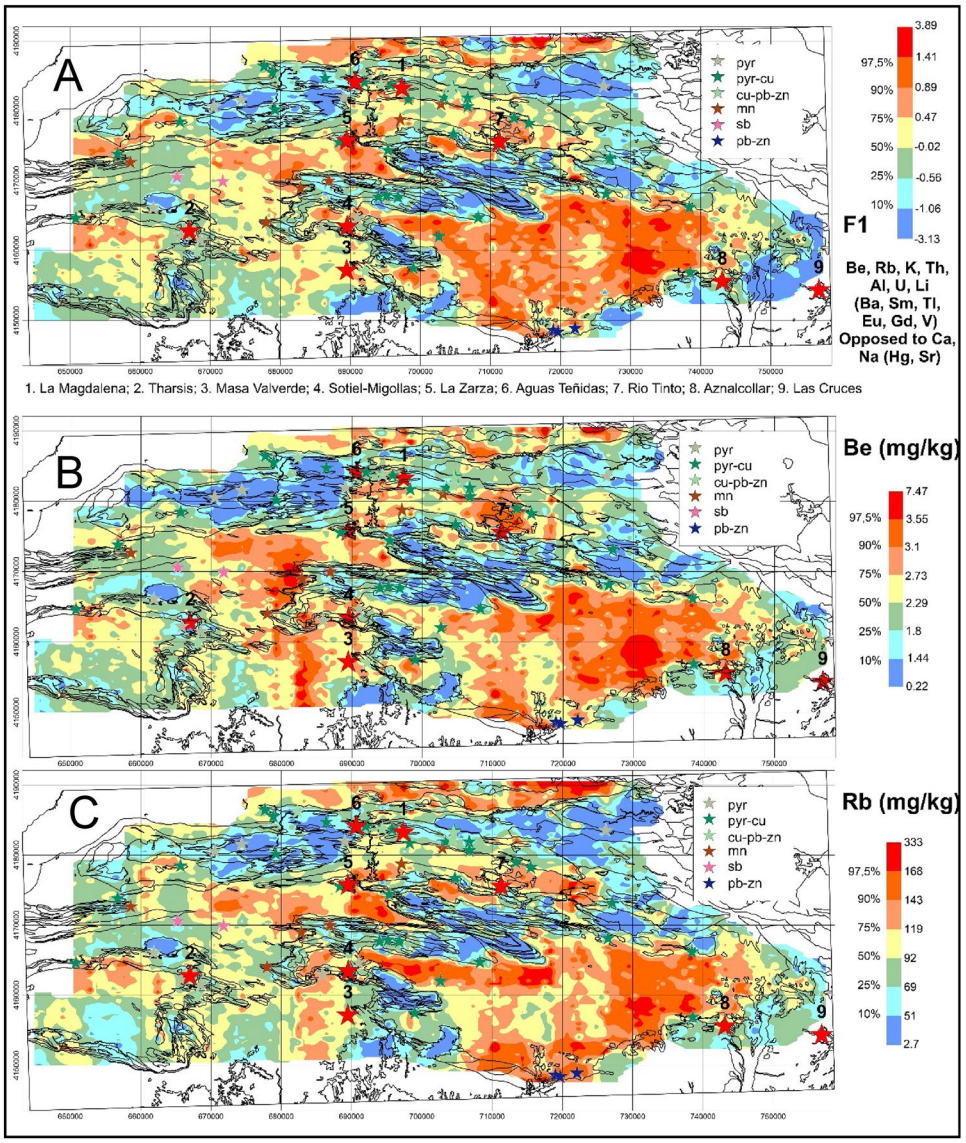

Fig. 7 **A** Factor scores distribution of element association F1: Be-Rb-K-Th-Al-U-Li-(Ba-Sm-Tl-Eu-Gd-V) in contrast to Ca-Na-(Mg-Sr). **B** Distribution contour map of Be. **C** Distribution contour map of Rb

We have used factorial analysis by main component extractions with "varimax rotation". Elements with loadings over 0.25 are considered representative members of each association resulting from the chosen factor model (Table 2).

The element association F1: Be-Rb-K-Th-Al-U-Li-(Ba-Sm-Tl-Eu-Gd-V) in contrast to Ca-Na-(Mg-Sr) accounts for 15.48% of data variability, and the F2 association: Er-Ho-Tm-Y-Yb-Dy-Lu-Tb-Gd-(Na) accounts for 15.11% of data variability; F3: Bi-Au-Sb-Ag-As-Sn-Pb-Ba-(S-Cu-Hg) and F4: Fe-S-Co-Cr-Ni-V-Al-Sr-(P-Ga-Mn-Li) account for 11.04% and 11,09% of data variability, while F5: Cd-Zn-S-Hg-(Cu-Pb-Tl-Ag-Sb-In-As) and F6: Sm-Nd-Pr-La-Eu-Ce-Gd-Tb-(Th-U) in contrast to (Na) account for 6.19% and 10.39% of data variability, respectively. In each association, elements are listed with decreasing loadings, and elements in brackets have loadings between 0.5 and 0.25.

The element association F1: Be-Rb-K-Th-Al-U-Li-(Ba-Sm-Tl-Eu-Gd-V) in contrast to Ca-Na-(Mg-Sr) show a spatial distribution with a litoestratigrafic control (Fig. 7). It's mostly controlled by the presence of soil developed on PQ group, but is important to differentiate between the east zone, in Valverde del Camino antiform with values up to 0.47, in contrast with La Puebla de Guzman antiform in the west part with values lower than 0.47, that could suggest differences in its origin and composition. Leistel et al. (1997) highlight the importance of good information in areas of PQ rocks in antiform core zones for mineral exploration. The PQ core of Puebla de Guzmán antiform can be considered as a nappe thrust over a substratum of VSC. Moreover, it shows high values related to Gil-Márquez granites and facies from Pulo do Lobo formation and Santa Barbara formation due to the presence of feldspars in shales, lithoarenites and feldespatic sandstones in these formations. The Culm Group

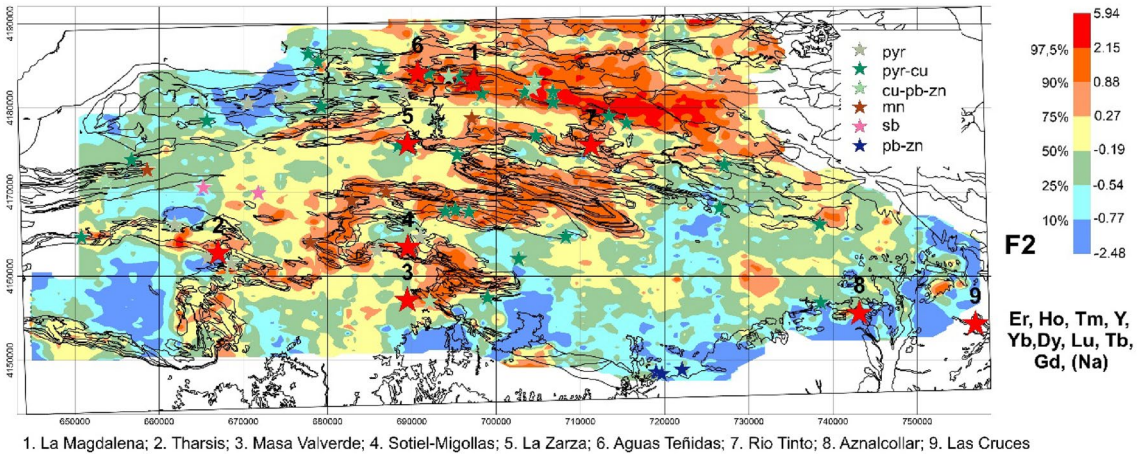

Fig. 8 Factor scores distribution of element association F2: Er-Ho-Tm-Y-Yb-Dy-Lu-Tb-Gd-(Na)

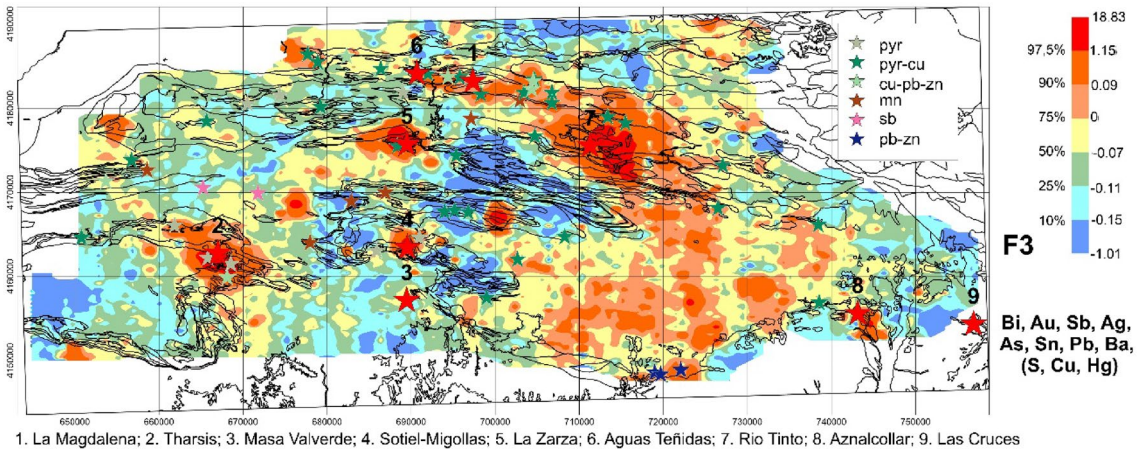

Fig. 9 Factor scores distribution of element association F3: Bi-Au-Sb-Ag-As-Sn-Pb-Ba-(S-Cu-Hg)

shows an erratic distribution for this factor, while both VSC and SNSB present a negative correlation.

This factor is similar to F2 in the total extraction of topsoils in Atlas Geoquímico de España (Locutura et al., 2012), that also shows higher values in the PQ Group to the eastern part of the IPB. This factor has a geochemical signature of more evolved granites, differentiating between Gil-Marquez granites and the rest of the granites of the SNSB due to their different origin (Castro et al., 1995). The higher values of the eastern zone of Valverde del Camino antiform suggest a possible sub-outcrop granite similar to Gil-Marquez granite. We can also observe these higher values in monoelemental contour maps like beryllium and rubidium (Fig. 7B, C.)

The element association F2: Er-Ho-Tm-Y-Yb-Dy-Lu-Tb-Gd-(Na) is formed mainly by HREE and Na. It is mostly related to igneous units (Fig. 8). This factor shows an essential relationship between the igneous rocks from the SNSB and the volcanic rocks from the VSC. This geochemical association confirms the idea that the Variscan rocks from the BSNS are the parental rocks of the volcanic materials from the VSC (Thiéblemont et al., 1997).

There are some differences between different the VSC. Higher values are related to E-W band of VSC (rhyolites and dacites) at the northeast part of the project. This factor is more related to acid terms that are also influenced by the erosion of the BSNS granites to the north. In contrast, VSC andesites (intermediate terms) at the northwest part of the project show lower values due to geochemical characteristics and because this zone does not influence the erosion of BSNS granites.

We can also see high values (up to 0.27) in the eastern part of PQ outcrops in Valverde del Camino antiform, possibly related to a sub-outcrop granite observed in F1.

The F3 factor: Bi-Au-Sb-Ag-As-Sn-Pb-Ba-(S-Cu-Hg) is a geochemical association with several elements related

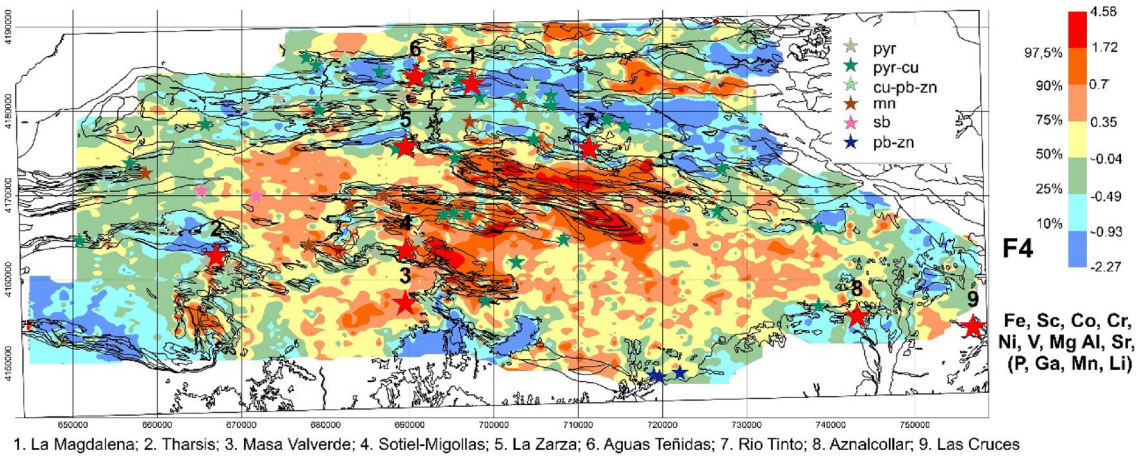

Fig. 10 Factor scores distribution of element association F4: Fe-S-Co-Cr-Ni-V-Al-Sr-(P-Ga-Mn-Li)

to the metallogenic process so associated with ore deposits (Fig. 9). It is an "ore factor." There are VMS ore deposits, gossans, and stockworks in the IPB, but some of the main elements in this group, like Bi, Au, and As are typical from stockwork associations (Leistel et al., 1997; Marcoux et al., 1996; Velasco et al., 2013).

The factor scores represent an irregular and erratic distribution controlled by the ore deposits. In detail, we can observe the higher values (from 0.09 to 18.83), related to Rio Tinto, not only related to VMS and stockwork but also with dumps and mining wastes in the surrounding areas of several open pits (Atalaya, Salomón, Dehesa, Lago) due to the contamination of the soil affected by sulfides extraction (López et al., 2008).

Similar to higher values around other ore deposits such as La Zarza and Tharsis that are also accompanied by stockworks (Tornos, 2006) and different high concentrations with maximum values which are not so high around ores with a description of stockworks; Sotiel-Migollas (Santos et al., 1996), Aguas Teñidas (Tornos, 2006), Aznalcollar (Pascual et al., 1996), Angostura and San Miguel (Tornos, 2006). Other "anomalies" unrelated to known ore deposits need follow-up studies to consider their importance in future mineral exploration.

The main geological units show no relevant correlation with this factor, so we can only remark on the geochemical difference between the two outcrops of the PQ Group in the different antiforms again.

The association F4: Fe-S-Co-Cr-Ni-V-Al-Sr-(P-Ga-Mn-Li) is explained by elements reflecting a lithological factor. This factor contains several ferromagnesian elements related to the geochemical signature of basic igneous rocks (Fig. 10). We can observe this association in the distribution of higher factor score values in soils developed on mafic

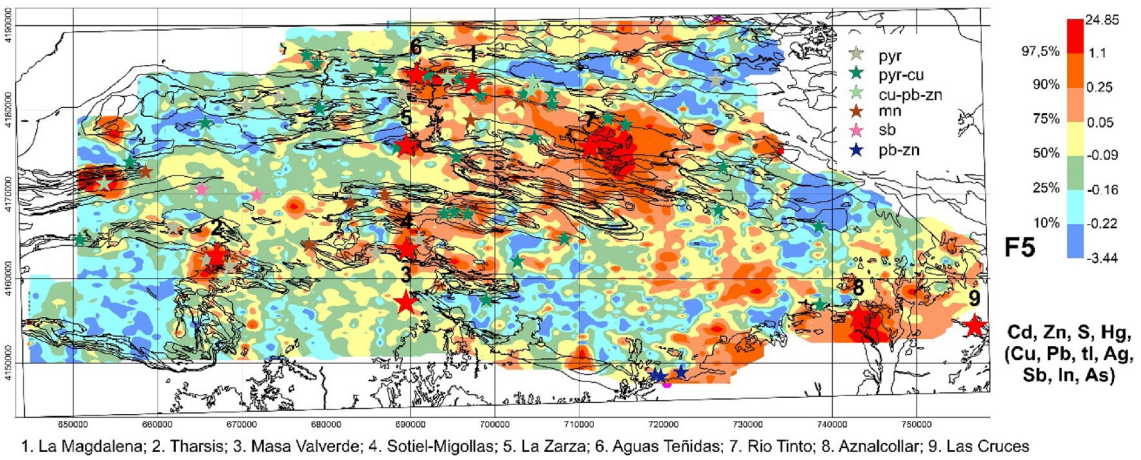

Fig. 11 Factor scores distribution of element association F5: Cd-Zn-S-Hg-(Cu-Pb-Tl-Ag-Sb-In-As)

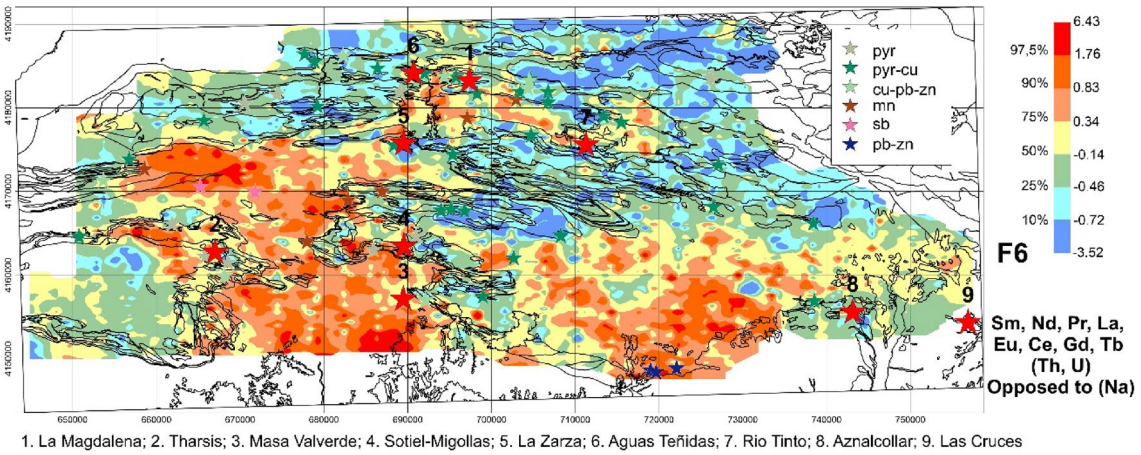

Fig. 12 Factor scores distribution of element association F6: Sm-Nd-Pr-La-Eu-Ce-Gd-Tb-(Th-U) in contrast to (Na)

rocks outcrops of Variscan terrains from the SNSB and primary facies from the VSC.

The elevated values of the factor scores in the VSC are explained by basalts that outcrops in the North and West factor of the Valverde and the Puebla de Guzman antiforms (from 1.72 to 4.58). Also, high values in Variscan igneous rocks are related to mafic compositions, mainly gabbros, diorites and cuarzodiorites at Northeast and small bodies of gabbros, micrograbros and diabases in El Berrocal, Sotiel and at South of Valverde del Camino village. Basaltic rocks in the IBP show high contents in Ni, Cr and Mg, elements present in this factor (Mitjavila et al., 1997).

We foreground the difference between the northern and the southern Culm Group. Matas et al. (2015) explain geological variations between this zone (undifferentiated Culm), in the north part with organic-rich black shales that could be also enriched in ferromagnesian elements and the other type of Culm in the south region.

The element association F5: Cd-Zn-S-Hg-(Cu-Pb-Tl-Ag-Sb-In-As) is characterized by elements that reflect a mineralization factor (Fig. 11). It shows several discrepancies with Factor 3. In this case, is a typical volcano-sedimentary geochemical association with Zn-Cd-Cu-Pb. However, some of these elements can present a specific geological control (Pb, Sb and Tl) and could appear in silicate minerals of igneous rocks.

Again, we can observe the highest concentration of values (from 1.1 to 24.85) around Rio Tinto ore deposits, like in factor 3. We can also see higher matters related to the same deposits, like factor 3: Tharsis, Sotiel, and La Zarza and other not observed so clearly like Aznalcollar, Aguas Teñidas and La Magdalena, with values up to 1.1. Different interesting high concentrations are related to some other small VMS ore deposits like Sierrecilla in the eastern part, a Zn deposit, Tinto y Santa Rosa and Cerro Buitron in the central region Lagunazo and San Telmo.

Like in factor 3, some high concentrations need future studies because they do not correlate with ore deposits.

Such as factor 1, we also noted the geochemical differences, between the Variscan rocks of the SNSB with low values of factor scores (from 0.05 to 3.44) and Gil-Marquez with high values (from 0.05 to 1.1), confirming the different origin (Castro et al., 1995).

The other main geological units do not show any particular relation with this factor except the sedimentary materials from the Gualdaquivir Basin in the southeastern part of the project, probably related to crops and the anthropic influence of agricultural fertilizers.

Finally, the F6 association Sm-Nd-Pr-La-Eu-Ce-Gd-Tb-(Th-U), in contrast to (Na), is mainly formed by light REE, and some related elements (Th and U). The elevated values of the factor scores of this association are related to the Culm Group, so these elements have an important affinity with the geological materials of these sandstones and shales in turbiditic sequences (Fig. 12).

There is also a correlation between this factor and materials from the PQ Group in the Valverde antiform. Although the lithological control is still being determined, we can again observe the difference between two PQ outcrops, as shown in factor 1.

5 Conclusion

Spatial distribution of chemical elements in the residual soils of the Iberian Pyrite Belt is determined by lithological and metalogenic factors, as well as a partial influence from mining wastes.

Firstly, although there are many studies regarding geology in the IPB, geochemical studies can help to improve the geological maps discriminating and differentiating between zones with similar geology, like both outcrops of the PQ Group that show a different geochemical affinity.

Also, these studies can help to uncover possible non-outcropped bodies like the likely granite in the southwest of Valverde antiform, detailed geophysical studies are proposed in this area to confirm this hypothesis.

Secondly, we could partially discriminate between this metallogenic province's different types of ore deposit characteristics. In addition, some high concentrations of factor scores from F3 and F5 are not related to already known ore deposits, some with high values of critical elements so that they could be new exploration targets for follow-up surveys in the future. This fact could limit the areas for future mining exploration.

Finally, this geochemical database and the factor analyses, combined with geological and geophysical information in GIS analyses, help build exploration models.

Acknowledgements This work has been possible thanks to the funds of the Spanish Geological Survey (IGME-CSIC) with an internal project to improve the geochemical knowledge of the Iberian Pyrite Belt. I would like to acknowledge M. Martinez and F.L. Sanz for the sampling and preparation, and ACTABS laboratories for the analyses and an excellent internal quality control. Finally, I would like to express my gratitude to two of my master degree college J. Velasco-Acebes and E. Marino for their revisions and advices.

Funding Open Access funding provided thanks to the CRUE-CSIC agreement with Springer Nature.

Data availability Data availability in Geoquímica - InfolGME.

Declarations

Conflict of interest There are no direct or indirect conflicts of interest between the authors and the work being submitted for publication in the journal.

References

Aguilar, J., Galán, E. & Gómez, J. (1999). *Estudio de elementos traza en Suelos de Andalucía*. Junta de Andalucía: https://www.juntadeandalucia.es/medioambiente/web/Bloques_Tematicos/Estado_Y_Calidad_De_Los_Recursos_Naturales/Suelo/Suelo.pdf.

Almodóvar, G. R., Yesares, L., Sáez, R., Toscano, M., González, F., & Pons, J. M. (2019). Massive sulfide ores in the Iberia Pyrite Belt: *Mineralogical and Textural evolution*. *Minerals, 9*(11), 653. https://doi.org/10.3390/min9110653

Barrie, T. C., Amelin, Y., & Pascual, E. (2002). U-Pb Geochronology of VMS mineralization in the Iberian Pyrite Belt. *Mineralium Deposita, 37*, 684–703. https://doi.org/10.1007/s00126-002-0302-7

Batista, M. J., Abreu, M. M., Locutura, J., De Oliviera, D., Matos, J. X., Silva, C., Bel-Lan, A., & Martins, L. (2012). Evaluation of trace elements mobility from solis to sediments between the Iberian Pyrite Belt and the Atlantic Ocean. *Journal of Geochemical Exploration, 123*, 61–68. https://doi.org/10.1016/j.gexplo.2012.06.011

Batista, M. J., Mateus, A., Matos, J. X., Gonçalves, M. A., Figueiras, J., Abreu, M. M., & Luz, F. (2020). Geochemical exploration and assessment of environmental impacts in the Portuguese sector of the Iberian Pyrite Belt. *Comunicaçoes Geologicas, 107*, 79–90.

Bonnemaision, M., Braux, C., Joubert, M. & Mercier, F. (1993). *Estudio de la gestión de multicriterios en la investigación de sulfuros polimetálicos: Herrerías, antiforme de Puebla de Guzmán.* SEIEMSA (Grupo BRGM).

Castro, A., De la Rosa, J. D., Fernández, C., & Moreno-Ventas, I. (1995). Unstable flow, magma mixing and magma-rock deformation in a deep-seated conduit: The Gil-Márquez Complex, southwest Spain. *Geologische Rundschau, 84*(2), 359–374. https://doi.org/10.1007/BF00260446

Darnley, A.G., Bjorklund, B., Boelviken, B., Gustavsson, N., Koval, P.V., Plant, J.A., Steenfelt, A., Tauchid, M. & Xuejing, X. (1995). *A global geochemical database for environmental and resource management.* Final Report of IGCP Project 259. UNESCO. ISBN 92-3-103085-X.

Demetriades, A., Reimann, C., & Filzmoser, P. (2014). Evaluation of GEMAS project quality control results. (Chapter 6). In C. Reimann, M. Birke, A. Demetriades, P. Filzmoser, & P. O'Connor (Eds.), *Chemistry of Europe's agricultural soils. Geologisches Jahrbuch (Reihe B102)* (pp. 47–60). Schweizerbarth.

Díez-Montes, A., & Bellido, F. (2008). Magmatismo TTG y Al-K en la Zona Surportuguesa. Relaciones entre plutonismo y vulcanismo. *Geo-Temas*, *10*, 1449–1452.

Díez-Montes, A., Bellido, F., Sánchez-García, T. (2011). TTG and Al-K magmatisms in the South Portuguese Zone. Relations between plutonism and volcanism. In *Seventh Hutton Symposium on Granites and Related Rocks* (p. 47).

Díez-Montes, A., Sánchez, A., Sánchez, T., Bellido, F. & García-Crespo, J. (2017). *Lithogeochemistry of volcanic rocks in the Río Tinto Mine, Iberian Pyrite Belt (Huelva, Spain)*. Instituto Geológico y Minero de España. ISBN: 978-84-9138-042-9.

Dunning, G. R., Díez-Montes, A., Matas, J., Martín-Parra, L. M., Almarza, J., & Donaire, M. (2002). Geocronología U/Pb del volcanismo ácido y granitoides de la Faja Pirítica Ibérica (Zona Surportuguesa). *Geogaceta, 32*, 127–130.

Fernández-Caliani, J. C., Barba-Brioso, C., González, I., & Galán, E. (2009). Heavy metal pollution in soils around the abandoned mine sites of Iberian Pyrite Belt (Southwest Spain). *Water, Air, and Soil Pollution, 200*, 211–226. https://doi.org/10.1007/s11270-008-9905-7

Fernández-Caliani, J. C., Romero-Baena, A., González, I., & Galán, E. (2020). Geochemical anomalies of critical elements (Be Co, Hf, Sb, Sc, Ta, V, W, Y and REE) in soils of western Andalusia (Spain). *Applied Clay Science*. https://doi.org/10.1016/j.clay.2020.105610

Galán, E., Fernández-Caliani, J. C., González, I., Aparicio, P., & Romero, A. (2008). Influence of geological setting on geochemical baselines of trace elements in soils. Application to soils of South-West Spain. *Journal of Geochemical Exploration., 98*(3), 89–106. https://doi.org/10.1016/j.gexplo.2008.01.001

García-Cortés, A. (2011). *Cartografía de recursos minerales de Andalucía*. IGME-Consejería de Economía, Innovación y Ciencia de la Junta de Andalucía.

Gonçalves, M. A., & Mateus, A. (2019). Delimiting geochemical anomalies in exploring covered deposits with multifractal methods and using stream sediment data from the Iberian Pyrite Belt, Southwest Iberia. *Ore Geology Reviews, 112*, 103018. https://doi.org/10.1016/j.oregeorev.2019.103018

Grunsky, E. C. (2010). The interpretation of geochemical survey data. *Geochemistry: Exploration, Environment, Analysis, 10*(1), 27–74. https://doi.org/10.1144/1467-7873/09-210

Gumiel, P., Sanderson, D. J., Arias, M., Roberts, S., & Martín-Izard, A. (2010). Analysis of the fractal clustering of ore deposits in the Spanish Iberian Pyrite Belt. *Ore Geology Reviews, 38*(4), 307–318. https://doi.org/10.1016/j.oregeorev.2010.08.001

IGME. (1982). *Síntesis geológica de la Faja Pirítica del SO de España*. Instituto Geológico y Minero de España.

Inverno, C., Díez-Montes, A., Rosa, C., García-Crespo, J., Matos, J., García-Lobón, J. L., Carvalho, J., Bellido, F., Castello-Branco, J. M., Ayala, C., Batista, M. J., Rubio, F., Grando, I., Tornos, F., Oliveira, J. T., Rey, C., Araujo, V., Sánchez-Garcia, T., Pereira, Z., … Sousa, P. (2015). Introduction and geological setting of the Iberian Pyrite Belt. In P. Weihed (Ed.), *3D, 4D and predictive modelling of major mineral belts in Europe. Mineral resource reviews.* Springer. https://doi.org/10.1007/978-3-319-17428-0_9

Julivert, M., Fontbote, J. M., Ribeiro, A. & Conde, I. (1974). *Mapa tectónico de la Península Ibérica y Baleares*. E: 1.1.000.009, IGME.

Kabata-Pendias, A. (2001). *Trace elements is soils and plants* (p. 315). CRC Press.

Leistel, J. M., Marcoux, E., Thiéblemont, D., Quesada, C., Sánchez, A., Almodóvar, G. R., Pascual, E., & Sáez, R. (1997). The volcanic-hosted massive sulphide deposits of the Iberian Pyrite Belt Review and preface to the Thematic Issue. *Mineralium Deposita, 33*, 2–30. https://doi.org/10.1007/s001260050130

Locutura, J. (2011). Descripción de las mineralizaciones de la Zona Sudportuguesa. In García-Cortés, A. (Ed.), *Cartografía de recursos minerales de Andalucía*, Madrid (p. 108).

Locutura, J., Bel-Lan, A., García-Cortés, A. & Martínez-Romero, S. (2012). *Atlas Geoquímico de España*.

López, M., González, I., & Romero, A. (2008). Trace elements contamination of agricultural soils affected by sulphide exploitation (Iberian Pyrite Belt, Sw Spain). *Environmental Geology, 54*, 805–818. https://doi.org/10.1007/s00254-007-0864-x

Luz, F., Mateus, A., Matos, J. X., & Goncalves, M. A. (2014). Copper, Zn and Pb soil geochemistry data from the NE domain of the Iberian Pyrite Belt in Portugal: implications for mineral exploration. *Geochemistry: Exploration, Environment, Analysis, 14*(4), 341–358. https://doi.org/10.1144/geochem2012-19

Mantero, E., Alonso-Chaves, F., Garcia-Navarro, E., Azor, A., Poblet, J., & Lisle, R. J. (2011). Tectonic style and structural analysis of the Puebla de Guzman Antiform (Iberian Pyrite Belt, South Portuguese Zone, SW Spain***). *Spec. Publ. Geol. Soc. Lond., 349*, 203–222. https://doi.org/10.1144/SP349.11

Marcoux, E., Moëlo, Y., & Leistel, J. M. (1996). Bismuth and cobalt minerals: Indicators of stringer zones to massive sulfide deposits, Iberian Pyrite Belt. *Mineralium Deposita, 31*, 1–26. https://doi.org/10.1007/BF00225392

Matas, J. (IGME), Martín-Parra, L. M. (IGME), Rubio Pascual, F. J. (IGME), Roldán, F. J. (IGME) & Martín-Serrano, A. (IGME). (2015). *Mapa Geológico 1:200.000. Sevilla-Puebla de Guzmán.*

Mielke, J. E. (1979). Composition of the earth´s crust and distribution of the elements. In Siegel, F. R. (Ed.), *Review of research of modern problems in International Association for Geochemistry and Cosmochemistry. Earth Science Series* No 16. UNESCO Report SC/GEO/544/3. (pp. 13–37).

Mitjavila, J., Martí, J., & Soriano, C. (1997). Magmatic evolution and tectonic setting of the Iberian Pyrite Belt volcanism. *Journal of Petrology, 38*, 727–755. https://doi.org/10.1093/petroj/38.6.727

Moreno, C. (1993). Postvolcanic paleozoic of the Iberian Pyrite Belt: An example of basin morphologic control on sediment distribution in a turbidite basin. *Journal of Sedimentary Research, 63*, 1118–1128. https://doi.org/10.1306/D4267CBC-2B26-11D7-8648000102C1865D

Munhá, J., Riberiro, A., Fonseca, P., Oliveira, J. T., Castro, P. & Quesada, C. (1989). Accreted terranes in Southern Iberia: Beja-Acebuches opjiolite and related oceanic sequences. In *28th International Geology Congress, Washington, USA. Abstract with programs, 2* (p. 481–482).

Pascual, E., Maestre, A., Pons, J. M., Sáez, R., Almodovar, G. R., & Toscano, M. (1996). Geoquímica de los halos de alteración hidrotermal relacionados com los yacimientos de sulfuros massivos de Aznalcóllar-Los Frailes: Criterios de evaluación de la intensidad de alteración. *Boletin Geológico y Minero., 107*(5), 551–557.

Pereira, Z., Matos, J. X., Fernandes, P., & Oliveira, J. T. (2008). *Palynostratigraphy and systematic palynology of the Devonian and Carboniferous successions of the South Portuguese Zone, Portugal* (p. 34). Memorias Geológicas.

Pinedo-Vara, I. (1963). *Piritas de Huelva*. In Summa, S. L. (Ed.).

Plant, J. A., Hale, M., & Rigdway, J. (1989). Developments in regional geochemistry for mineral exploration. *Transactions of the Institutions of Mining and Metallurgy, Section B: Applied Earth Science, 97*, B116–B140.

Quesada, C. (1991). Geological constraints on the Paleozoic tectonic evolution of tectonostratigraphic terranes in the Iberian Massif. *Tectonophysics, 185*, 145–225. https://doi.org/10.1016/0040-1951(91)90446-Y

Quesada, C. (1996). Estructura del sector español de la Faja Pirítica: Implicaciones para la exploración de yacimientos. *Boletín Geológico y Minero, 107*(3–4), 65–78.

Reimann, C. (2005). Geochemical mapping: Technique or art? *Geochemistry: Exploration, Environment, Analysis, 5*(4), 359–370. https://doi.org/10.1144/1467-7873/03-051

Reimann, C., Filzmoser, P., & Garrett, R. (2002). Factor analysis applied to regional geochemical data: Problems and possibilities. *Applied Geochemistry, 17*, 185–206. https://doi.org/10.1016/S0883-2927(01)00066-X

Rosa, C., McPhie, J., & Relvas, J. (2010). Type of volcanoes hosting the massive sulfide deposits of the Iberian Pyrite Belt. *Journal of Volcanology and Geothermal Research., 194*(4), 107–126. https://doi.org/10.1016/j.jvolgeores.2010.05.00

Routhier, P., Aye, P., Boyer, F., Lécolle, M., Moliere, E.P., Picot, P. & Roger, G. (1978). *La Ceinture Sud-Ibérique à amas sulfurés dans sa partie espagnole mediane*, Mém BRGM. editions

Salminen, R. (Chief-editor), Batista, M. J., Bidovec, M., Demetriades, A., De Vivo, B., De Vos, W., Duris, M., Gilucis, A., Gregorauskiene, V., Halamic, J., Heitzmann, P., Lima, A., Jordan, G., Klaver, G., Klein, P., Lis, J., Locutura, J., Marsina, K., Mazreku, A., O'Connor, P. J., Olsson, S. Å., Ottesen, R.-T., Petersell, V., Plant, J. A., Reeder, S., Salpeteur, I., Sandström, H., Siewers, U., Steenfelt, A. & Tarvainen, T. (2005). *Geochemical Atlas of Europe, FOREGS.*

Salminen, R., Tarvainen, T., Demetriades, A., Duris, M., Fordyce, F. M., Gregorauskiene, V., Kahelin, H., Kivisilla, J., Klaver, G., Klein, H., Larson, J. O., Lis, J., Locutura, J., Marsina, K., Mjartanova, H., Mouvet, C., O´Connor, P., Odor, L., Ottonello, G.,

Paukola, T., Plant, J. A., Reimann, C., Schermann, O., Siewers, U., Steenfeelt, A., Van der Sluys, J., de Vivo, B. & Williams, L. (1998). *FOREGS geochemical mapping. Field manual*. Geologian tutkimuskeskus, Opas - Geological Survey of Finland, Guide 47. 36 pages, 15 figures, and 1 appendix.

Santos, A., Caballero, B., & Prada, J. M. (1996). Descripción geológica de los yacimientos de Sotiel Coronada. *Boletin Geológico y Minero, 107*(5), 511–518.

Schermerhorn, L. (1971). An outline stratigraphy of the Iberian Pyrite Belt. *Boletin Geológico y Minero, 82*, 238–268.

Schutz, W., Ebeneth, J., & Meyer, K. D. (1987). Trondhjemites, tonalities and diorites in the South Portughese Zone and their reactions to the vulcanites and mineral deposits of the Iberian Pyrite Belt. *Geologische Rundschau, 76*, 201–212.

Silva, J. B., Oliveira, J. T., Ribeiro, A. (1990). Structural Outline, South Portuguese Zone, In R. D. Dallmeyer, E. Martínez García (Eds.) *Pre-MesozoicGeology of Iberia*, Springer-Verlag, pp. 348–362.

Strauss, G. K., & Madel, J. (1974). Geology of massive sulphide deposits in the Spanish-Portuguese Pyrite Belt. *Geol Rundsch, 63*, 191–211. https://doi.org/10.1007/BF01820984

Taylor, S. R. (1964). The abundance of chemical elements in the continental crust: A new table. *Geochimica Et Cosmochimica Acta, 28*, 1273–1278. https://doi.org/10.1016/0016-7037(64)90129-2

Thiéblemont, D., Pascual, E., & Stein, G. (1997). Magmatism in the Iberian Pyrite Belt: Petrological constraints on a metallogenic model. *Mineralium Deposita, 33*, 98–110. https://doi.org/10.1007/s001260050135

Tornos, F. (2006). The environment of formation and styles of volcanogenic massive sulfides: The Iberian Pyrite Belt. *Ore Geology Reviews., 28*(3), 259–307. https://doi.org/10.1016/j.oregeorev.2004.12.005

Velasco, F., Herrero, J. M., Suárez, S., Yusta, I., Alvaro, A., & Tornos, F. (2013). Supergene features and evolution of gossans capping massive sulfide deposits in the Iberian Pyrite Belt. *Ore Geology Reviews., 53*, 181–203. https://doi.org/10.1016/J.OREGEOREV.2013.01.008

WRB. (2014). The world reference base for soil resources 2014. In *International soil classification system for naming soils and creating legends for soil maps*. World Soil Resources Reports 106. FAO. http://www.fao.org/3/i3794en/I3794en.pdf.

Yesares, L., Saéz, R., Nieto, J. M., Ruiz de Almodovar, G., Gómez, C., & Escobar, J. M. (2015). The Las Cruces deposit, Iberian Pyrite Belt, Spain. *Ore Geology Reviews., 66*, 25–46. https://doi.org/10.1016/j.oregeorev.2014.10.019

Zuo, R., Wang, J., Xiong, Y., & Wang, W. (2021). The processing methods of geochemical exploration data: Past, present, and future. *Applied Geochemistry, 132*, 105072. https://doi.org/10.1016/j.apgeochem.2021.105072